MOLECULAR IMAGING AND BIOLOGY

Mol Imaging Biol (2019) 21:269–278
DOI: 10.1007/s11307-018-1238-3

Published Online: 25 June 2018

RESEARCH ARTICLE

In Vivo Evaluation of Magnetic Targeting in Mice Colon Tumors with Ultra-Magnetic Liposomes Monitored by MRI

Caroline J. Thébault,[1,2,3,4,5] Grégory Ramniceanu,[1,2,3,4] Aude Michel,[5] Claire Beauvineau,[1,2,3,4] Christian Girard,[1,2,3,4] Johanne Seguin,[1,2,3,4] Nathalie Mignet,[1,2,3,4] Christine Ménager,[5] Bich-Thuy Doan[1,2,3,4]

[1]*Chimie ParisTech, Unité de Technologies Chimiques et Biologiques pour la Santé (UTCBS), PSL Research University, 75005, Paris, France*
[2]*CNRS, UMR 8258, UTCBS, 75006, Paris, France*
[3]*Sorbonne-Paris-Cité, UTCBS, Université Paris Descartes, 75006, Paris, France*
[4]*INSERM, U 1022, UTCBS, 75006, Paris, France*
[5]*UPMC Univ Paris 06, CNRS UMR 8234, Laboratoire PHENIX, Case 51, Sorbonne Universités, 4 place Jussieu, 75005, Paris, France*

Abstract

Purpose: The development of theranostic nanocarriers as an innovative therapy against cancer has been improved by targeting properties in order to optimize the drug delivery to safely achieve its desired therapeutic effect. The aim of this paper is to evaluate the magnetic targeting (MT) efficiency of ultra-magnetic liposomes (UML) into CT26 murine colon tumor by magnetic resonance imaging (MRI).

Procedures: Dynamic susceptibility contrast MRI was applied to assess the bloodstream circulation time. A novel semi-quantitative method called $\%I_{0.25}$, based on the intensity distribution in T_2^*-weighted MRI images was developed to compare the accumulation of T_2 contrast agent in tumors with or without MT. To evaluate the efficiency of magnetic targeting, the percentage of pixels under the intensity value $I_{0.25}$ ($I_{0.25} = 0.25(I_{max} - I_{min})$) was calculated on the intensity distribution histogram.

Results: This innovative method of processing MRI images showed the MT efficiency by a $\%I_{0.25}$ that was significantly higher in tumors using MT compared to passive accumulation, from 15.3 to 28.6 %. This methodology was validated by *ex vivo* methods with an iron concentration that is 3-fold higher in tumors using MT.

Conclusions: We have developed a method that allows a semi-quantitative evaluation of targeting efficiency in tumors, which could be applied to different T_2 contrast agents.

Key words: MRI, Magnetic targeting, Magnetic nanoparticle, Liposome, Image analysis method, Tumor

Introduction

The last decades have witnessed significant advances on cancer treatment. Chemotherapy still remains the major cancer treatment despite its high toxicity. Recent growth of

Electronic supplementary material The online version of this article (https://doi.org/10.1007/s11307-018-1238-3) contains supplementary material, which is available to authorized users.

Correspondence to: Christine Ménager; *e-mail:* christine.menager@upmc.fr, Bich-Thuy Doan; *e-mail:* bich-thuy.doan@chimie-paristech.fr

nanomedicine has enabled the development of new nanocarriers for the delivery of drug to their targeting sites and/or triggered features in order to release its properties [1]. The goals of nanocarriers are to improve the benefit to its risk ratio, by increasing the drug accumulation in the tumor, decreasing its accumulation in healthy organs and by the delivery of the therapeutic molecule preferentially to their targeted area [2]. Nanocarriers can be liposomes, nanoparticles, polymers, micelles, or antibodies, just to name a few [3]. Among the various nanocarriers, liposomes represent a versatile drug carrier matching high biocompatibility with their ability to enclose polar drugs in their inner aqueous cavities and hydrophobic or non-polar therapeutic payloads in their lipid bilayers [4]. Due to their functional versatility, liposomes thus remain the most intensively investigated delivery vector. A first strategy to selectively target tumor cells is to graft ligands or antibodies to the liposomal surface. Physical approach is an alternative and complementary approach, which consists in non-invasive magnetic targeting (MT) in order to guide and accumulate magnetic nanomaterials in selected tissues or cells by applying an external magnetic field gradient. Liposomes have been investigated for encapsulating magnetic nanoparticles and several drugs as for instance, doxorubicin, anti-infectious, antiestrogen, and myorelaxants [5].

The strategies that would allow magnetic nanoparticles encapsulation within liposomes have been developed mainly for tracking *via* magnetic resonance imaging (MRI) [4, 6] and magnetic targeting [7–9]. For this last purpose, the main issue is to achieve a high degree of loading in order to obtain an important magnetization of the liposomes. We have recently proposed an alternative method to standard thin film hydration process that consists in evaporation of a reverse emulsion (water in oil) that enables a higher internal aqueous loading of magnetic nanoparticles (almost a 100-fold). Due to their high magnetic payload, ultra-magnetic liposomes (UML) were able to accumulate in solid tumors *via* the application of an external magnet [8, 10].

The control of the nanocarrier biodistribution is essential for the development of nanomedicine. The advantage of UML is dual as they can be followed by MRI and guided by using a magnet. MRI is the modality of choice as it is non-invasive and provides quantitative 3D data with high contrast. Spatial and temporal pharmacokinetics can be easily performed in order to monitor the *in vivo* biodistribution of diagnostic or therapeutic vectors in organs. This pharmacokinetic is especially important to check the vector stealthiness property that is required to increase tumor accumulation [11]. Several MRI methods based on their relaxation rates R_2 and R_2* measurements are developed to quantify the iron content in tissues such as the liver, but the quantification remains a challenge because these relaxometry-based techniques are sensitive to the physiopathological status of the tissue, to the iron particle size, and to the magnetic field B_0 heterogeneity [12].

The aim of this paper is to propose a new method to evaluate the magnetic targeting efficiency of UML in xenografted murine colon tumors. For this purpose, an original *in vivo* MRI method of image analysis was developed. The results were compared to *ex vivo* analysis: iron titration and confocal microscopy observation.

Material and Methods

Materials

1,2-Dipalmitoyl-sn-glycero-3-phosphocholine (DPPC), 1,2-distearoyl-sn-glycero-3-phosphocholine (DSPC), and 1,2-distearoyl-sn-glycero-3-phosphoethanolamine-*N*-[amino(polyethylene glycol)-2000] (ammonium salt) (DSPE-PEG2000) were purchased from Avanti Polar lipids, Inc. Cy5.5-NHS ester was purchased from Interchim (Montluçon, France). The CT26 murine colon carcinoma cell line (ATCC, CRL-2638), the BNL 1ME A.7R.1 (ATCC, TIB-75) murine normal epithelial liver cell line, and the NIH/3T3 murine fibroblasts cell line (ATCC, CRL-1658) were purchased from American Type Culture Collection (LGC Standards, Molsheim, France). Extravidin-peroxydase was purchased from Sigma-Aldrich. Alamar Blue was supplied from Thermo Fisher Scientific.

MNP Synthesis and UML Preparation

Magnetic nanoparticles (MNP) of maghemite (γ-Fe_2O_3) were synthetized according to Massart's procedure [13], detailed in Electronic Supplementary Material (ESM), and redispersed at 1 M of iron in injection buffer (0.11 M NaCl, 0.02 M sodium citrate, and 0.01 M HEPES) for *in vivo* experiments.

UML was prepared by reverse phase evaporation method as described by Béalle et al. [8] and detailed in the ESM.

To synthetize fluorescent UML, cyanine 5.5-NHS esther was grafted to DSPE-PEG_{2000}-NH_2 according to Jarzyna et al. [14] (ESM).

Iron was quantified by atomic absorption spectroscopy after degradation of UML in 37 % HCl.

Physicochemical Characterizations

MNP and UML were observed by transmission electron microscopy (TEM) and UML by CryoTEM. UML diameters were measured by tunable resistive pulse sensing (TRPS) on a qNano system (Izon Science, Oxford, UK).

To evaluate the volume fraction of MNP per UML, the magnetophoretic mobilities of liposomes were measured in a magnetic field gradient of 195 T/m [15]. Three independent experiments, each tracking 50 UML, were performed to evaluate the average UML velocity. The balance between the magnetic force and the viscosity one was applied on liposomes to allow the calculation of the magnetic load.

MRI System

Relaxivity measurements were performed on a 7 T vertical spectrometer fitted with an ultra-shielded refrigerated magnet (300WB, Bruker, Avance II, Wissembourg, France) and equipped with an RF birdcage coil with a 40-mm inner diameter (Bruker) and a nominative 200 mT m^{-1} actively shielded gradient coil. The shimming protocol was performed using an optimized combined shimming directions available from our 10 shims micro-imaging system, adapted to our micro-MRI spectrometer and the 40-mm diameter Bruker RF probe.

For *in vivo* MRI experiments, animals were anesthetized with 1.5 % isoflurane gas in an air/O_2 mixture (0.5 and 0.2 l/min, respectively).

Relaxivity Measurement

Samples of MNP and UML were diluted in injection buffer (0.108 M NaCl, 0.02 M sodium citrate and 0.01 M HEPES) at various concentrations of iron (0.01, 0.05, 0.10, 0.20, 0.50 mM). *In vitro* relaxivity experiments were carried out by recording T_2 and T_1 maps. The Paravision 5 software allowed the recordings with the following parameters: for T_1 map: RARE images; TE = 13 ms; TR = 15, 8, 3, 1.2, 0.800, 0.594, 0.300, 0.144, 0.050, and 0.033 s, RARE factor 2; for T_2 map: multi-echo MSME images: Hermitian pulse, TR/TE = 15 s/11 ms, 32 echoes. Fields of view of 3×3 cm^2, matrix size of 128×64, and slice thickness of 1.5 mm were used for T_1 and T_2 maps. Relaxation times T_1 and T_2 of each sample were calculated by fitting the T_1-weighed and T_2-weighed signal intensity S with the relation $S_{TR} = A + B(1\text{-}\exp(-TR/T_1)$ and $S_{TE} = A + B.\exp.(-TE/T_2)$. Molar relaxivities r_1 and r_2 were obtained using the following equation $\frac{1}{T_i} = r_i[Fe] + \frac{1}{T_{i,0}}$ with i: 1 or 2.

Cytotoxicity Assay

The cytotoxicity was determined on CT26 tumor cells, TIB-75 hepatocytes, and NIH/3T3 fibroblasts using the Alamar Blue test as described in the ESM.

Animals

Studies were carried out on 7-week-old Balb/C female mice (Janvier, St Genest de Lisle, France). Animal experiments were conducted according to European and National guidelines and were approved by the institutional ethics committee (CEEA34.JS.142.1). *In vivo* experiments presented in this work required 62 animals.

In vivo Liver Uptake by MRI

To visualize the capture of UML by the liver, a dynamic susceptibility contrast (DSC) imaging methodology was used: IntraGateFLASH (Fast Low Angle Shot gradient echo sequence with IntraGate) images were recorded to suppress breath motion artifacts. IntraGate module patented by Bruker is a self-gating sequence based on a retrospective image reconstruction by sorting out the MRI signal between the breath peaked motions [16, 17]. It was used in a cine mode with 1-min duration and adapted time resolution accordingly to the uptake and clearance behavior of the ULMs: Hermitian pulse, TR/TE = 90 ms/3 ms, 52 repetitions. Field of view of 3×3 cm^2, matrix size of 256×256, for a 117 µm in plane resolution, and 5 slices distant of 3 mm with a thickness of 1.088 mm were used. After three reference acquisitions, 100 µl of MNP or UML at 5 mM iron concentration in injection buffer were injected using a 30-G catheter previously placed in the caudal vein of the animal. The mouse was monitored by MRI for 1 h after injection with 1-min time resolution, and then points were taken at 2 and 4 h and at different times for a week to detect the clearance. For each time, a region of interest (ROI) was drawn for the liver and for the water phantom tube located near the mouse into the field of view. The signal of these two ROI was determined using the ImageJ software (National Institutes of Health, Bethesda). The signal of the liver was then normalized with the phantom signal and reported for each time point after normalization by the precontrast value. The GraphPad 6 software allowed the fitting of the signal *versus* time curves using nonlinear regression (bell-shaped fitting).

Ectopic Tumor Implantation

Two weeks after implantation, a mouse bearing a subcutaneous CT26 tumor was sacrificed. The tumor was removed, submerged in DMEM culture medium and cut in 30-mm^3 fragments. For the implantation, the mouse lateral flank above the posterior paws was disinfected using alcohol, and the tumor fragments were transferred into sterile PBS and inserted subcutaneously using a 12 gauge trocar into the two mouse flanks sides above the posterior paws [18].

In vivo Magnetic Targeting Studied by MRI

Whole tumors as reference were imaged with the following sequence: FLASH images: Hermitian pulse, TR/TE = 350 ms/5 ms, $\alpha = 40°$, triggered on respiration. Field of view of 3×3 cm^2, matrix size of 256×256 corresponding to 177 µm × 117 µm in plane resolution, and 15 to 17 slices with a thickness of 1 mm were used, for an acquisition time of about 7 min. The animal was removed from the MRI apparatus, and a catheter (30 G) was placed in its caudal vein. Magnetic targeting was achieved through two

cylindrical magnets (NdFeB, with diameter 6 mm × 2 mm thickness, 0.35 T, Supermagnete, Germany) that were stuck together and positioned on the skin over the tumor; the other contralateral tumor was taken as the control without magnetic targeting. UML (100 µl at 100 mM in iron) were injected through the catheter, and the animal was kept in this position for 30 min. Then, the magnets were removed and post-targeting MRI images of tumors were acquired. The animals were then sacrificed.

Data Processing

For the data processing, MRI image of each slice was opened in the ImageJ software (National Institutes of Health, Bethesda) using the plugin BrukerOpener, the ROI corresponding to the tumor was drawn, and the pixel intensity distribution was obtained. The pixel intensity distributions for each slice of the tumor were compiled using MATLAB software (R2015a, Natick, Massachusetts, United States) to obtain a pixel intensity distribution for the whole tumor. The percentage of pixels under the $I_{0.25}$ value was then calculated ($I_{0.25} = 0.25*(\text{Intensity}_{max} - \text{Intensity}_{min})$) with the same software (Script in the ESM). To compare the reference tumor and tumors with or without magnetic guidance, percentages of pixels under the $I_{0.25}$ for each condition were averaged, and a statistic Mann-Whitney test was performed using GraphPad 6.

ICP Analysis

After harvest, iron was quantified from tumors, liver, spleen, kidneys, and lungs by ICP-AES (Inductively Coupled Plasma-Atomic Emission Spectrometry) as described in ESM.

Biphotonic and Confocal Microscopy

The fluorescence intensity of tumors after injection of fluorescent UML with or without magnetic targeting was measured *ex vivo* by using biphotonic and confocal microscopies as described in the ESM.

Results

Characterization of UML

Magnetic nanoparticles (MNP) of maghemite (γ-Fe_2O_3) were sorted by size, and the fraction with the higher mean diameter ($d_0 = 9.8$ nm; $\sigma = 0.37$) was chosen to acquire a greater magnetization (ESM). The particles were stabilized by complexation with citrate molecules and dispersed in an aqueous buffer (0.108 M NaCl, 0.02 M sodium citrate and 0.01 M HEPES) at pH 7 for all the *in vivo* experiments. Ultra-magnetic liposomes (UML) and fluorescent UML were prepared by reversed phase evaporation process (REV) [8]. After magnetic separation to eliminate non-encapsulated MNP, the iron concentration of UML was measured by flame ICP spectrometry. TEM observation confirmed that the UML were filled with MNP (Fig. 1a). The presence of the bilayer has been confirmed by cryoTEM proving the formation of unilamellar liposomes (ESM). Dynamic light scattering (DLS) was not appropriate to characterize UML encapsulating MNP since the mean diameter reflects both MNP and UML sizes. Moreover, since the refractive index of both nano-objects was different, the values were not relevant. Therefore, tunable resistive pulse sensing (TRPS) method [19] was used for the measurement of UML diameters. As the liposome size was obtained by counting each individual liposome that went through a calibrated pore, both diameter and number of UML could be obtained (Fig. 1b). The availability of membranes with the TRPS method that starts with nanopores at 50 nm does not allow this technique to measure the MNP. According to a log-normal law, the mean diameter was determined at 230 nm with a 0.2 polydispersity.

In order to determine the amount of MNP per UML, magnetophoresis experiments were carried out. The velocity of UML submitted to a magnetic field gradient was measured. Therefore, volume fraction of MNP per UML can be calculated to counterbalance the forces applied between viscosity and magnetic forces applied on UML [15]. With a mean velocity of 37.6 µm/s in a 195 T/m magnetic field gradient, the volume fraction of MNP in UML was 24 % which indicates that about 3100 MNP were encapsulated per UML ($6.1.10^{-15}$ g of Fe/UML). The molecular ratio of Fe/lipid was calculated as 83 (mol/mol), which is higher than data reported in literature (0.53 mol Fe/mol lipid [20], 19 mol Fe/mol lipid [21], 0.15 mol Fe/mol lipid [22]). This high MNP loading is crucial to achieve magnetic targeting. Indeed, the magnetic force F_{mag} depends on the UML magnetic moment and thus on the number of MNP entrapped in the liposome.

Relaxivities in solution were measured at 7 T for MNP and UML, and they were compared to Cliavist®, a commercial iron oxide MRI contrast agent. The values of longitudinal and transverse relaxivities r_1 and r_2 are given for these three types of objects in Table 1. Iron oxide nanoparticles are well-known for their contrast agent properties in T_2-weighted MR Imaging. They give a hyposignal in appropriate T_2-weighted MRI acquisition sequences. The UML transverse relaxivity r_2 increases compared to the one of free MNP. Indeed, once there is compartmentalization in liposomes, cooperating MNP give a higher magnetic moment resulting in a higher proton spin dephasing with shortened T_2 value [23]. UML relaxivities are therefore suitable for *in vivo* contrast agent use with a better r_2/r_1 of 150 compared to 78 for the commercial Cliavist® and 35 for free MNP. Taking into consideration the difference of r_2 values between free MNP and UML, we

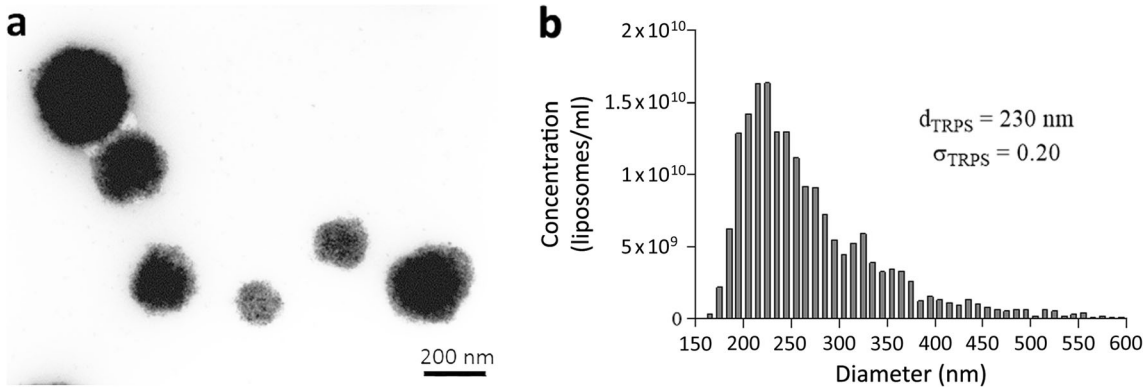

Fig. 1. **a** TEM picture of UML. **b** UML size distribution measured by TRPS.

used relaxivity measurements to evaluate the stability of UML over time. A stable r_2 value reflecting the UML stability in RPMI was observed for at least 5 h (ESM).

In order to confirm that these UML were appropriate for intravenous injections, cytotoxicity tests were performed in this RPMI medium. Viabilities of CT26 (colon tumor), TIB-75 (hepatocyte), and NIH/3T3 (fibroblast) cells were evaluated using increasing concentrations of UML. The absence of UML toxicity at iron concentration under 10 mM for tumor and fibroblast cells, and a low toxicity for hepatocyte cells, was observed as illustrated in Fig. 2. From the stability and toxicity results, we considered that *in vivo* injections were conceivable.

In vivo Liver Uptake

In vivo biodistribution studies were then performed to characterize the kinetic behavior of the UML in mice and, in particular, to assess the stealthiness property of UML after intravenous injection. To ascertain tumor magnetic targeting, the UML must indeed circulate within a certain time into the bloodstream before being eliminated by Kupffer cells and captured by the liver and spleen as expected from their size. The dynamic susceptibility contrast MR imaging at 7 T allowed the following of the hepatic uptake by kinetic acquisitions. These acquisitions can be specifically adjusted every minute for the first hour and sequentially for a week to obtain the whole process of nanoparticle elimination: liver uptake and degradation [11]. Figure 3 summarizes the kinetic of capture and clearance of MNP and UML with examples of MRI images illustrating the evolution of signal *versus* time at each specific point (1: initial signal, 2: decreasing slope, 3: plateau, 4: increasing signal). The UML and MNP uptake by the liver resulted in a decrease of MRI signal in the liver up to a minimum. To obtain a match between this minimum of signal and the maximum of liver uptake, 5 mM of iron was injected as previously determined by Ramniceanu et al. [11]. Indeed, with a higher concentration of iron, the MRI signal in the liver saturated, preventing the visualization of the minimum value corresponding to the maximum uptake by the liver. After a plateau of a few days, the signal increased corresponding to the liver clearance.

From hundred nanometer size of nanocarriers, a very fast hepatic capture was expected. In our case, the PEG corona around UML membrane allowed an improvement of the circulation time [1]. Indeed, the minimum of signal corresponding to the total uptake of UML by the liver was measured at 1 h after injection. Furthermore, after 10 min, the signal intensity was at 50 % between its minimum and maximum, meaning that a significant part of the UML was still circulating, although there is no linear correlation but an exponential correlation between the MRI intensity and the MNP concentration. Therefore, the circulation duration in the bloodstream and within the tumor vascular network was

Table 1. Relaxivity values of MNP, UML, and Cliavist® in solution at 7 T

	MNP	UML	Cliavist®
r_1 (mM^{-1} s^{-1})	2.2	1.5	1.3
r_2 (mM^{-1} s^{-1})	77	225	202
r_2/r_1	35	150	78

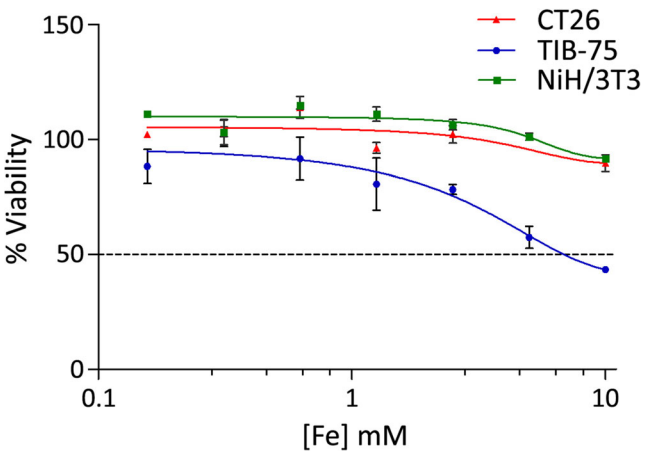

Fig. 2. Viability of CT26 (colon tumor), TIB-75 (hepatocyte), and NIH/3T3 (fibroblast) as a function of iron concentration after 1-h incubation with UML.

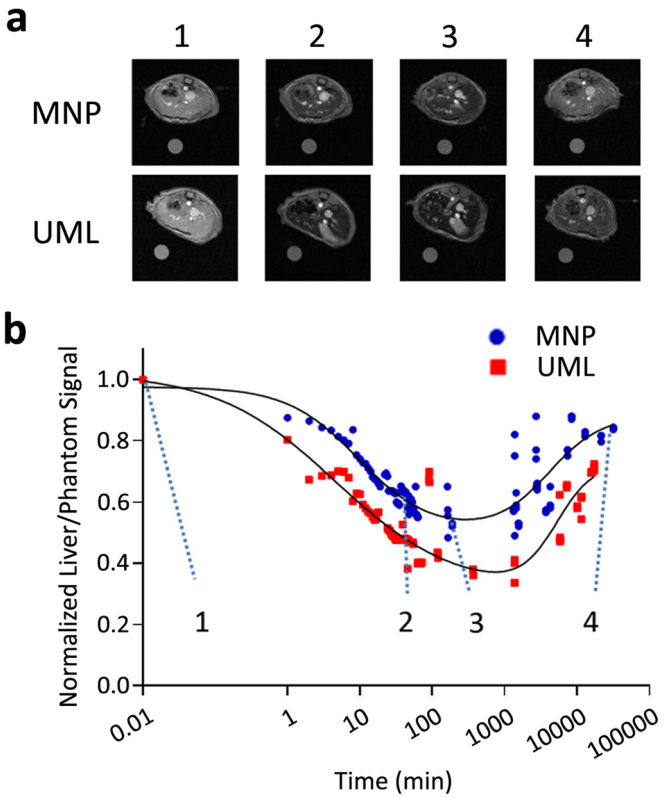

Fig. 3. MRI kinetic visualization of liver uptake, and liver clearance after intravenous injection of MNP or UML. **a***In vivo* IntraGateFLASH MRI images of the liver before and at 30 min, 120 min, and 15 days after injection of MNP or UML. **b** Kinetic curves of hepatic uptake after intravenous injection of MNP (blue) or UML (red) with three animals involved in each group. Lines connecting points are a guide for the eye.

about 30 min during which the magnetic targeting can be expected to be efficient. The difference of minimum T_2^*-weighted MRI signal value between MNP and UML is due to the difference of transverse relaxivity r_2.

In vivo Magnetic Targeting

MT efficiency was investigated on mice with bilateral CT26 murine tumors implanted on each flank. After a T_2^*-weighted MRI image acquisition pre-injection, two superimposed magnets were positioned on one of the tumors and UML were injected intravenously. The magnetic field at the surface was 0.35 T and then decreased exponentially according to the following equation: $B = 0.354e^{-0.41d} - 0.004$ with B the magnetic field in Tesla and d the distance from magnets in mm. To compare the passive accumulation of UML in tumors due to enhanced permeability retention (EPR) effect and the effect of MT, magnets were removed after 30 min and a T_2^*-weighted MRI image was acquired.

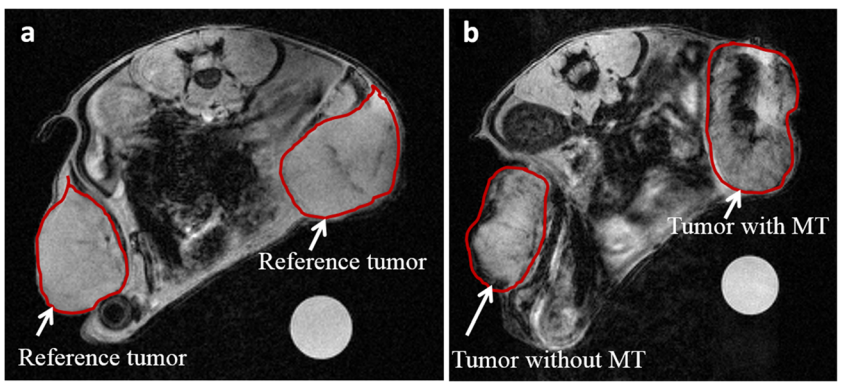

Fig. 4. *In vivo* T_2^*-weighted MRI images of CT26 tumors **a** before and **b** after UML injection with and without magnetic targeting (MT).

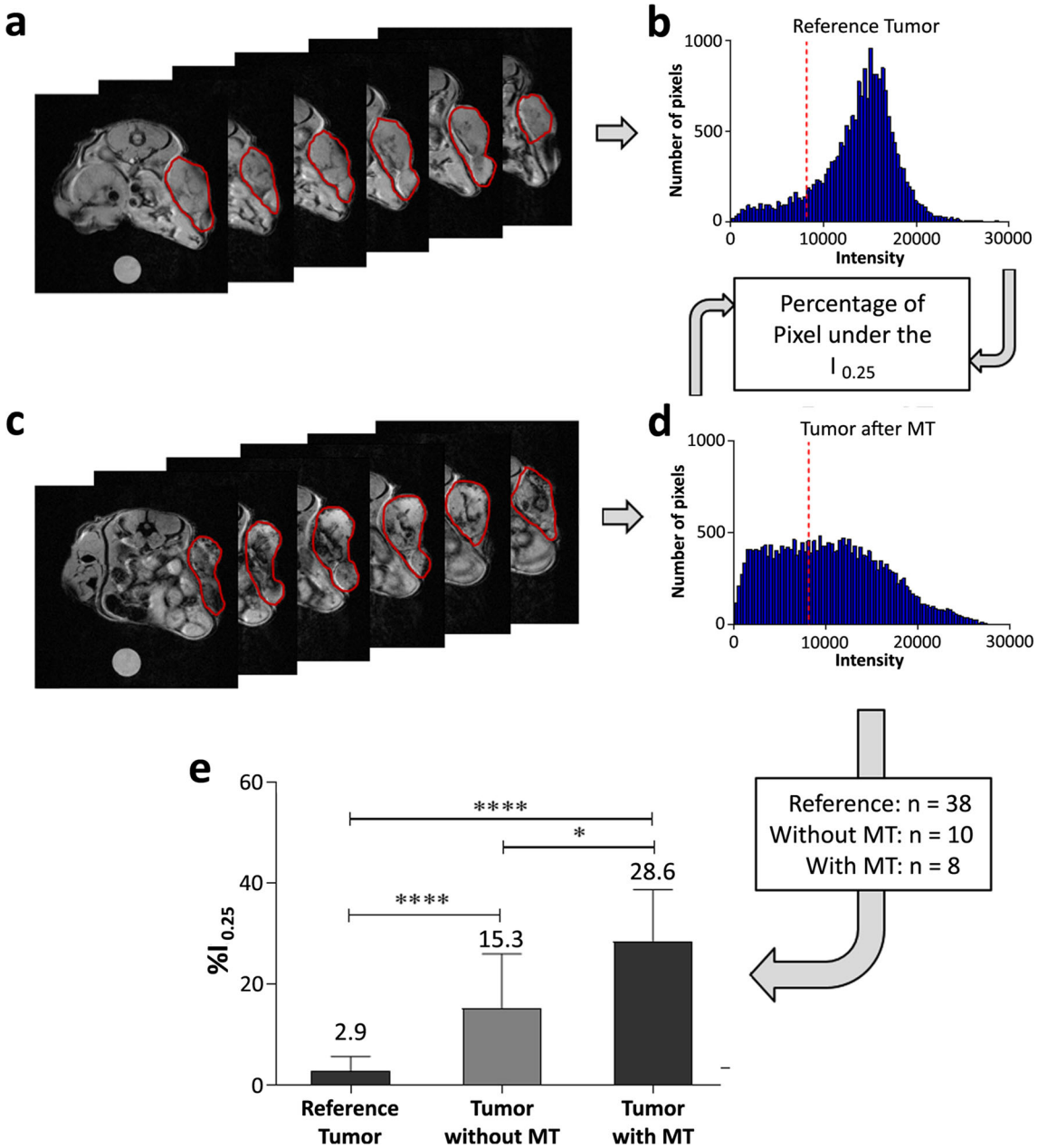

Fig. 5. $\%I_{0.25}$ methodology of data processing from the T_2^*-weighted MRI images for evaluation of *in vivo* UML accumulation in tumors. **a** Tumor before injection. **b** MRI intensity distribution associated to the tumor before injection. **c** Tumor after UML injection. **d** MRI intensity distribution associated to the tumor after UML injection and magnetic targeting (MT). **e** Summary of percentage of pixels under $I_{0.25}$ on MRI tumor images. Non-gaussian distribution Mann-Whitney test: $^*P < 0.05$; $^{**}P < 0.01$; $^{***}P < 0.001$; $^{****}P < 0.001$; ns $P > 0.5$.

Figure 4 shows an example of pre- and post-injection images. The difference of accumulation was observed with a higher hyposignal in the tumor using MT.

To evaluate the *in vivo* increase of UML accumulation in tumors, from MT, a post-processing methodology called $\%I_{0.25}$ was developed. Regions of interest (ROI) were drawn on each slice of the tumor on MRI images (Fig. 5a, c), and the pixel intensity distribution was obtained for each slice. The compilation of these distributions gave a single pixel intensity distribution per tumor as shown in Fig. 5b, d.

The mean signal in T_2^*-weighted images did not show significant differences between tumors injected with UML with MT (9375 u.a. ± 1017) or without MT (10,335 u.a. ± 1868). Then, the percentage of pixels under the $I_{0.25}$ ($0.25(\text{Intensity}_{max} - \text{Intensity}_{min})$) for tumors before and after injection, with or without MT, was compared (Fig. 5e). This

parameter was chosen as the UML presence as T_2 contrast agent induced a shift in the intensity distribution toward low-intensity values. A significant difference was obtained between non-injected mice and injected mice, 2.9 and 15.3 %, respectively. This reflected the passive accumulation of UML in these highly vascularized tumors [24]. More interestingly, the active accumulation correlated to magnetic targeting showed a significant increase as referred to UML-injected mice, meaning a net gain when compared to passive accumulation. A 28.6 % of the pixels were under the $I_{0.25}$ in the case of MT active accumulation compared to 15.3 % (*) for the passive accumulation.

This methodology of data treatment from signal distribution allowed the analysis of non-homogenous MRI signal on which global intensity average is not significant enough for the *in vivo* monitoring of magnetic nanoparticles. Therefore, this methodology can be used to compare diverse targeting methods with other T_2 nanocarriers and different tumor types.

Ex vivo Magnetic Targeting

The accumulation of fluorescent UML (cyanine 5.5 labeled lipids) in tumors can be checked *ex vivo* by confocal microscopy and iron titration (ESM). The signal measured from tumors with MT (12.10^5) was significantly higher (**) than the signal from tumors with passive accumulation ($8.4.10^5$). Furthermore, *ex vivo* ICP measurements performed on tumors revealed a 3-fold increase of the iron accumulation in tumors with MT (13.6 µg/g of tumor) as compared to tumors without MT (3.8 µg/g of tumor). The increase in both the iron and the lipid concentrations in the targeted tumors suggested that the UML were well preserved during their circulation.

Ex vivo experiments confirmed results obtained *in vivo* with MRI data treatment and *in vivo* monitoring methodology. Therefore, the comparison of various targeting techniques can be accomplished *in vivo* by using nanoparticles with T_2 MRI contrast agent properties and MRI monitoring.

Discussion

The quantitative evaluation of a targeting efficiency still remains a challenge. To solve this problem, chemists have to develop carriers/nanoparticles that can be detected by various imaging modalities. However, only few imaging modalities provide an absolute quantitative evaluation. Positron emission tomography (PET) is probably the most powerful method because radiotracers allow absolute quantification of the uptake of the positron emitting radiopharmaceuticals with high sensitivity, and the detection limit is in the picomolar range. Magnetic nanoparticles and magnetic systems have already been conjugated with PET radiotracers [25]. However, the strategies rely on the incorporation of a specific chelator inside or on the surface of nanoparticles involving constraints related to the manipulation of radioactive species. These systems are not competitive with existing clinical protocols [26–28]. Computed tomography is also well-known for its quantitative feature for perfusion *in vivo* using CT contrast agents like Ultravist and iodine. This modality is ionizing and requires a compromise between patient dose and signal-to-noise ratio [29]. *In vivo* optical imaging lacks the accurate quantitative feature as light scattering and quenching problems occur, and this requires image processing reconstruction to correct tissue absorption [30]. This is why the development of new methodologies that enable the evaluation of magnetic targeting efficiency is crucial.

MRI is a non-invasive, non-ionizing, quantitative, highly contrasted, and resolved imaging modality. However, although quantitation has already been demonstrated to be efficient with Gadolinium contrast agents, an image processing method has to be developed for iron oxide quantification [31]. Other authors have proposed *in vivo* quantification methods to access the accumulation of MNP in the tumor. One technique was to calculate the signal decay rate and the relative standard deviation (or relative dispersion) from T_2 maps to evaluate the heterogeneous distribution of MNP in the tissue [32]. An alternative was to consider the percentage change of the initial relaxivity value dR_2 [33]. Choudhury et al. proposed to segment hyposignals induced by the accumulation of MNP in different tumors to take into account the signal variability of the tumor type [34]. They proposed a processing method based on local contrast levels with the calculation of a fraction of the local mean signal intensity which was function of the tumor, and they suppressed the regions of natural hyposignal for the calculation of iron oxide nanoparticles uptake.

Quantitative susceptibility mapping (QSM) is a method [35] provided from 3D multi-echo sequence, to obtain a quantitative map of susceptibility. The susceptibility is proportional to the iron concentration. It was applied in our present data, but the QSM-MEDI reconstruction algorithm was sensitive to the required high 3D isotropic resolution of the quantitative 3D GE image, and no significative difference between the QSM maps with and without magnetic targeting was observed (data not shown). The $\%I_{0.25}$ appeared to be more robust and easy to use to provide evidence on the magnetic targeting of the UML.

In the present study, we have developed an original method that allowed a semi-quantitative evaluation of targeting efficiency in tumors, a method that could be applied for different T_2 contrast agents compared to the EPR effect. This method is based on the modification of the intensity distribution in standard T_2*-weighted images, easy to set up in all MRI facility and with short acquisition time. The MNP provided a hyposignal inducing a shift of the intensity histogram toward the low-intensity region. Therefore, we chose the percentage of pixels under the $I_{0.25}$ as the relevant parameter to quantify the increase of MNP accumulation. As our processing method compared pre-

with post-contrast injection images at 1-h period acquisition, it could be used in different kinds of tumors with low necrotic features.

Magnetic targeting appears as an alternative and attractive method of targeting compared to active targeting (with ligands). Préat et al. showed, for example, a percentage of injected dose in tumor 2-fold higher with MT than with $\alpha_v\beta_3$ integrin active targeting using RGD [36].

We demonstrated that UML combine two properties on the same object. The first one concerns MT, and the UML are very good candidates for MT according to the high concentration of MNP in their core. The second one is a very efficient T_2 MRI contrast agent feature useful to monitor their biodistribution. As shown in this work, UML have a circulation time of about 1 h allowing their accumulation into the tumors that can be used for future therapeutic purpose.

At this stage, it would be a particular interest to encapsulate and be able to release actively drugs which will be able to diffuse due to its low molecular weight. Thanks to the ability of liposomes to allow the encapsulation of hydrophilic or hydrophobic drugs, UML can be considered for theranostic. Indeed, several authors have shown the liposomal co-encapsulation of doxorubicin with iron oxide nanoparticles [37], Gd chelates [38], or the encapsulation of a hydrophobic sensitizer with iron oxide nanoparticles [39].

Conclusion

A novel semi-quantitative method based on the intensity distribution in MRI T_2^*-weighted images was developed to compare *in vivo* the accumulation of T_2 contrast agent. This method was perfectly adapted to evaluate the magnetic targeting efficiency of ultra-magnetic liposomes in CT26 colon tumors. Confocal microscopy and ICP were used as *ex vivo* techniques to validate this intensity distribution approach. Compared to active targeting, MT is versatile because it does not depend on the biological target and is also very easy to handle and cheap. Finally, these UML can be easily designed for theranostic applications.

Acknowledgements. This work was supported by the LabEx MiChem part of French state funds managed by the ANR within Le *Programme* Investissements d'Avenir under reference ANR-11-IDEX-0004-02. *In vivo* imaging was performed at the Life Imaging Facility of Paris Descartes University (LIOPA from the Plateform Imageries du Vivant – PIV) and partly supported by CNRS and ENSCP, ANR LightLab program.
We are grateful to Institut Français Weizmann for a postdoctoral grant (GR), Emmanuel Aubry from ALIPP6 for ICP analysis, Claire Wilhelm for magnetophoresis experiments, Cellular Imaging facility Imagic of Institut Cochin for confocal microscopy, and to Jean-Michel Guigner for CryoTEM.

Compliance with Ethical Standards

Conflict of Interest

The authors declare that they have no conflict of interest.

References

1. Shi J, Kantoff PW, Wooster R, Farokhzad OC (2016) Cancer nanomedicine: progress, challenges and opportunities. Nat Rev Cancer 17:20–37
2. Mura S, Nicolas J, Couvreur P (2013) Stimuli-responsive nanocarriers for drug delivery. Nat Mater 12:991–1003
3. Lammers T, Aime S, Hennink WE, Storm G, Kiessling F (2011) Theranostic nanomedicine. Acc Chem Res 44:1029–1038
4. Soenen SJ, Velde GV, Ketkar-Atre A, Himmelreich U, de Cuyper M (2011) Magnetoliposomes as magnetic resonance imaging contrast agents. Wiley Interdiscip Rev Nanomed Nanobiotechnol 3:197–211
5. Pattni BS, Chupin VV, Torchilin VP (2015) New developments in liposomal drug delivery. Chem Rev 115:10938–10966
6. Amstad E, Kohlbrecher J, Müller E et al (2011) Triggered release from liposomes through magnetic actuation of Iron oxide nanoparticle containing membranes. Nano Lett 11:1664–1670
7. Mikhaylov G, Mikac U, Magaeva AA, Itin VI, Naiden EP, Psakhye I, Babes L, Reinheckel T, Peters C, Zeiser R, Bogyo M, Turk V, Psakhye SG, Turk B, Vasiljeva O (2011) Ferri-liposomes as an MRI-visible drug-delivery system for targeting tumours and their microenvironment. Nat Nano Technol 6:594–602
8. Béalle G, Di Corato R, Kolosnjaj-Tabi J et al (2012) Ultra magnetic liposomes for MR imaging, targeting, and hyperthermia. Langmuir 28:11834–11842
9. Marie H, Lemaire L, Franconi F, Lajnef S, Frapart YM, Nicolas V, Frébourg G, Trichet M, Ménager C, Lesieur S (2015) Superparamagnetic liposomes for MRI monitoring and external magnetic field-induced selective targeting of malignant brain tumors. Adv Funct Mater 25:1258–1269
10. Fernandez-Sanchez ME, Barbier S, Whitehead J et al (2015) Mechanical induction of the tumorigenic β-catenin pathway by tumour growth pressure. Nature 523:92–95
11. Ramniceanu G, Doan BT, Vezignol C, Graillot A, Loubat C, Mignet N, Berret JF (2016) Delayed hepatic uptake of multi-phosphonic acid poly(ethylene glycol) coated iron oxide measured by real-time magnetic resonance imaging. RSC Adv 6:63788–63800
12. Hernando D, Levin YS, Sirlin CB, Reeder SB (2014) Quantification of liver iron with MRI: state of the art and remaining challenges. J Magn Reson Imaging 40:1003–1021
13. Massart R (1981) Preparation of aqueous magnetic liquids in alkaline and acidic media. IEEE Trans Magn 17:1247–1248
14. Jarzyna PA, Skajaa T, Gianella A, Cormode DP, Samber DD, Dickson SD, Chen W, Griffioen AW, Fayad ZA, Mulder WJM (2009) Iron oxide core oil-in-water emulsions as a multifunctional nanoparticle platform for tumor targeting and imaging. Biomaterials 30:6947–6954
15. Wilhelm C, Gazeau F, Bacri JC (2002) Magnetophoresis and ferromagnetic resonance of magnetically labeled cells. Eur Biophys J 31:118–125
16. Heijman E, de Graaf W, Niessen P, Nauerth A, van Eys G, de Graaf L, Nicolay K, Strijkers GJ (2007) Comparison between prospective and retrospective triggering for mouse cardiac MRI. NMR Biomed 20:439–447
17. Bovens SM, te Boekhorst BC, den Ouden K et al (2011) Evaluation of infarcted murine heart function: comparison of prospectively triggered with self-gated MRI. NMR Biomed 24:307–315
18. Seguin J, Doan BT, Latorre Ossa H, Jugé L, Gennisson JL, Tanter M, Scherman D, Chabot GG, Mignet N (2013) Evaluation of nonradiative clinical imaging techniques for the longitudinal assessment of tumour growth in murine CT26 colon carcinoma. Int J Mol Imaging 2013:1–13
19. Weatherall E, Willmott GR (2015) Applications of tunable resistive pulse sensing. Analyst 140:3318–3334
20. Martina MS, Fortin JP, Ménager C, Clément O, Barratt G, Grabielle-Madelmont C, Gazeau F, Cabuil V, Lesieur S (2005) Generation of superparamagnetic liposomes revealed as highly efficient MRI contrast agents for in vivo imaging. J Am Chem Soc 127:10676–10685
21. Bulte JWM, de Cuyper M, Despres D, Frank JA (1999) Preparation, relaxometry, and biokinetics of PEGylated magnetoliposomes as MR contrast agent. J Magn Magn Mater 194:204–209
22. Lorenzato C, Oerlemans C, van Elk M, Geerts WJC, Denis de Senneville B, Moonen C, Bos C (2016) MRI monitoring of

nanocarrier accumulation and release using gadolinium-SPIO co-labelled thermosensitive liposomes: Gd-TSM for nanocarrier localization and monitoring of release using MRI. Contrast Media Mol Imaging 11:184–194
23. Larsen BA, Haag MA, Serkova NJ, Shroyer KR, Stoldt CR (2008) Controlled aggregation of superparamagnetic iron oxide nanoparticles for the development of molecular magnetic resonance imaging probes. Nanotechnology 19:265102
24. Seguin J, Nicolazzi C, Mignet N, Scherman D, Chabot GG (2012) Vascular density and endothelial cell expression of integrin alpha v beta 3 and E-selectin in murine tumours. Tumor Biol 33:1709–1717
25. Malinge J, Géraudie B, Savel P, Nataf V, Prignon A, Provost C, Zhang Y, Ou P, Kerrou K, Talbot JN, Siaugue JM, Sollogoub M, Ménager C (2017) Liposomes for PET and MR imaging and for dual targeting (magnetic field/glucose moiety): synthesis, properties, and in vivo studies. Mol Pharm 14:406–414
26. Seo JW, Zhang H, Kukis DL, Meares CF, Ferrara KW (2008) A novel method to label preformed liposomes with ^{64}Cu for positron emission tomography (PET). Imaging. Bioconjug Chem 19:2577–2584
27. Petersen AL, Binderup T, Rasmussen P, Henriksen JR, Elema DR, Kjær A, Andresen TL (2011) ^{64}Cu loaded liposomes as positron emission tomography imaging agents. Biomaterials 32:2334–2341
28. Phillips WT, Goins BA, Bao A (2009) Radioactive liposomes. Wiley Interdiscip Rev Nanomed Nanobiotech 1:69–83
29. Klotz E, König M (1999) Perfusion measurements of the brain: using dynamic CT for the quantitative assessment of cerebral ischemia in acute stroke. Eur J Radiol 30:170–184
30. Pesnel S, Akkoul S, Ledée R, Leconge R, Pillon A, Kruczynski A, Harba R, Lerondel S, le Pape A (2011) Use of an image restoration process to improve spatial resolution in bioluminescence imaging. Mol Imaging 10:446–452
31. Haacke EM, Brown RW, Thompson MR, et al. (2014) Magnetic properties of tissues: theory and measurement. In: Magnetic resonance imaging: Physical Principles and Sequence Design. Ed. John Wiley & Sons. New York: Wiley-Liss, pp 741–779
32. Oakes JM, Breen EC, Scadeng M, Tchantchou GS, Darquenne C (2014) MRI-based measurements of aerosol deposition in the lung of healthy and elastase-treated rats. J Appl Physiol 116:1561–1568
33. Chertok B, Moffat BA, David AE, Yu F, Bergemann C, Ross BD, Yang VC (2008) Iron oxide nanoparticles as a drug delivery vehicle for MRI monitored magnetic targeting of brain tumors. Biomaterials 29:487–496
34. Melemenidis S, Jefferson A, Ruparelia N, Akhtar AM, Xie J, Allen D, Hamilton A, Larkin JR, Perez-Balderas F, Smart SC, Muschel RJ, Chen X, Sibson NR, Choudhury RP (2015) Molecular magnetic resonance imaging of angiogenesis in vivo using polyvalent cyclic RGD-Iron oxide microparticle conjugates. Theranostics 5:515–529
35. Wang Y, Liu T (2015) Quantitative susceptibility mapping (QSM): decoding MRI data for a tissue magnetic biomarker: QSM. Magnet Reson Med 73:82–101
36. Schleich N, Po C, Jacobs D, Ucakar B, Gallez B, Danhier F, Préat V (2014) Comparison of active, passive and magnetic targeting to tumors of multifunctional paclitaxel/SPIO-loaded nanoparticles for tumor imaging and therapy. J Control Release 194:82–91
37. Chen J, Ke X, He Z et al (2012) A MSLN-targeted multifunctional nanoimmunoliposome for MRI and targeting therapy in pancreatic cancer. Int J Nanomedicine 7:5053–5065
38. de Smet M, Heijman E, Langereis S, Hijnen NM, Grüll H (2011) Magnetic resonance imaging of high intensity focused ultrasound mediated drug delivery from temperature-sensitive liposomes: an in vivo proof-of-concept study. J Control Release 150:102–110
39. Di Corato R, Béalle G, Kolosnjaj-Tabi J et al (2015) Combining magnetic hyperthermia and photodynamic therapy for tumor ablation with Photoresponsive magnetic liposomes. ACS Nano 9:2904–2916